An Automatically Mode-Matched MEMS Gyroscope With Wide and Tunable Bandwidth

Soner Sonmezoglu, Said Emre Alper, and Tayfun Akin

***Abstract*— This paper presents the architecture and experimental verification of the automatic mode-matching system that uses the phase relationship between the residual quadrature and drive signals in a gyroscope to achieve and maintain matched resonance mode frequencies. The system also allows adjusting the system bandwidth with the aid of the proportional-integral controller parameters of the sense-mode force-feedback controller, independently from the mechanical sensor bandwidth. This paper experimentally examines the bias instability and angle random walk (ARW) performances of the fully decoupled MEMS gyroscopes under mismatched (∼100 Hz) and mode-matched conditions. In matched-mode operation, the system achieves mode matching with an error <10-ppm/Hz frequency separation between the drive and sense modes in this paper. In addition, it has been experimentally demonstrated that the bias instability and ARW performances of the studied MEMS gyroscope are improved up to 2.9 and 1.8 times, respectively, with the adjustable and already wide system bandwidth of 50 Hz under the mode-matched condition. Mode matching allows achieving an exceptional bias instability and ARW performances of 0.54°/hr and 0.025°/$\sqrt{}$hr, respectively. Furthermore, the drive and sense modes of the gyroscope show a different temperature coefficient of frequency (TCF) measured to be −14.1 ppm/°C and −23.2 ppm/°C, respectively, in a temperature range from 0 °C to 100 °C. Finally, the experimental data indicate and verify that the proposed system automatically maintains the frequency matching condition over a wide temperature range, even if TCF values of the drive and sense modes are quite different. [2013-0183]**

***Index Terms*— MEMS gyroscope, gyroscope, mode-matching, closed-loop control, force-feedback.**

I. Introduction

THE DEVELOPMENT of the MEMS technology brings an increase in the number of potential application areas of various types of microsensors, including microfluidics, communications, and aerospace, by providing an opportunity for the creation of miniaturized mechanical sensors in a microscopic scale. Among these, MEMS gyroscopes constitute one of the fastest growing segments in the sensor market relative to the fiber optic and ring laser gyroscopes, thanks to their high reliability, promising performance, small size, and low cost [1].

Over the last decade, there is a significant improvement appeared in the mechanical design of the MEMS gyroscopes. Resulting designs improve the performance of the gyroscope by achieving larger drive-mode vibration amplitudes, minimizing the undesired mechanical cross-talk between the resonance modes of the gyroscope, and using high-aspect ratio fabrication techniques [2]–[4]. Among MEMS gyroscope designs, the most investigated gyroscopes are the vibratory rate gyroscopes. Generally, the structure of a typical micromachined vibratory rate gyroscope has at least 2-DOF (degree-of-freedom) motion capability to achieve a Coriolis induced energy transfer between two separate resonance modes (drive and sense). The resonance frequency of these modes can be either mismatched or matched to each other (almost 0 Hz frequency difference between the drive and sense modes). It is a known fact that matching the drive and sense mode frequencies amplifies the rate sensitivity of the sense mode by its mechanical quality factor, which can be as high as few thousand in a vacuum ambient [5]. The increase in the rate sensitivity improves the signal-to-noise ratio (SNR) of the sensor. Therefore, the resonance mode frequencies of the gyroscope must be matched to reach an ultimate MEMS gyroscope performance One of the challenges of this approach is to keep the resonance frequencies matched over the operational temperature range, as the advantages of mode-matching instantly disappears at different operating temperatures.

Various approaches have been introduced in the literature to reduce the frequency mismatch between the resonance modes. Some approaches utilize localized thermal stress [6], whereas some other approaches use post-fabrication tuning of resonance masses with the help of selective polysilicon deposition [7] or laser trimming [8]. All of the above methods require a manual tuning effort, which is not desirable for mass-production and also may not be stable in time and for different operating temperatures. A more effective approach is to automatically tune the resonance mode frequencies of the gyroscope by an adjustable DC potential, which relies on the effect of electrostatic spring softening [9]–[11]. This method allows closed-loop automatic frequency control provided that there exists continuous information about the resonance frequency of the sense mode. This is possible either by intentionally introducing a square wave dither signal as a quadrature error into the gyroscope and checking its phase across the resonator of the gyroscope [9], or by injecting out-of-band pilot tones into the sense electrodes and checking the

Manuscript received June 7, 2013; revised October 15, 2013; accepted November 16, 2013. Date of publication February 11, 2014; date of current version March 31, 2014. This work was supported by the State Planning Organization of Turkey under Project titled Industrial Micro-Electro-Mechanical Systems. Subject Editor G. K. Fedder.

S. Sonmezoglu and S. E. Alper are with the MEMS Research and Applications Center, Middle East Technical University, Ankara 06531, Turkey (e-mail: sonmezoglusoner@gmail.com; said@metu.edu.tr).

T. Akin is with Department of Electrical and Electronics Engineering, Middle East Technical University, Ankara 06531, Turkey (e-mail: tayfun-akin@metu.edu.tr).

Color versions of one or more of the figures in this paper are available online at http://ieeexplore.ieee.org.

Digital Object Identifier 10.1109/JMEMS.2014.2299234

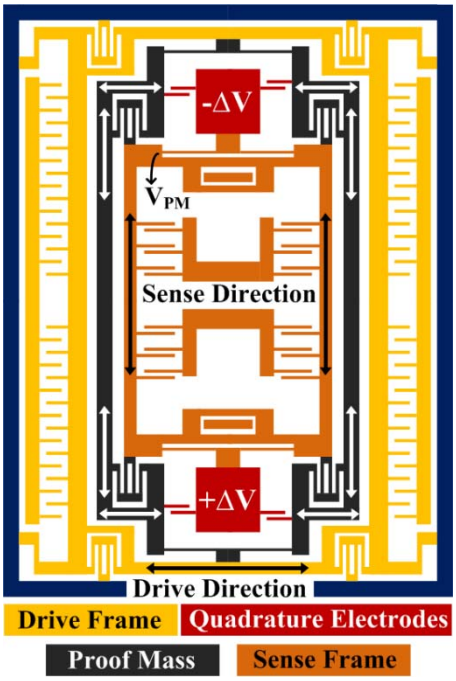

Fig. 1. Simplified structural view of the fully-decoupled MEMS gyroscope studied in this work.

amplitude difference between the tones [10], or by monitoring the amplitude of the residual quadrature signal [11]. Neither of these methods simultaneously achieves a high performance and wide bandwidth.

This paper proposes a method that substantially suppresses the electronic noise of the sense mode electronics and achieves sub-degree per-hour performance without sacrificing the system bandwidth [12], where the system bandwidth is kept wide with the pole-zero cancellation method as used in our group previously [13]. Compared to [12], this paper provides additional experimental and simulation data that describe the mode-matching method in more detail, presents new performance data obtained with a higher drive-mode vibration amplitude, and also shows that the proposed method is quite robust against temperature variations. The experimental data presented in this paper shows that the proposed mode-matching method allows the frequency matching condition to be automatically maintained over a wide temperature range, even for the case when the drive and sense mode TCFs are quite different from each other, making the proposed automatic mode-matching system ideal for the high end of tactical grade applications.

II. Proposed Mode-Matching System

Fig. 1 shows a simplified structural view of the fully-decoupled MEMS gyroscope studied in this work. The gyroscope structure consists of three suspended frames: the drive, proof mass, and sense frames. The drive and sense frames can vibrate along only one direction (1-DOF), whereas the proof mass frame vibrates along two orthogonal directions (2-DOF) to achieve Coriolis coupling between the drive and sense frames. Although the mechanical design theoretically eliminates the coupling between the drive and sense modes completely, fabrication imperfections can lead to an undesired mechanical cross-talk between these modes, which is named as the quadrature error. In the proposed gyroscope design, the quadrature error is cancelled by DC potentials, whose amplitudes are automatically-adjusted with the help of dedicated closed-loop quadrature cancellation electronics, applied to the quadrature nulling electrodes [14]. Despite the quadrature nulling, a finite amount of quadrature signal always exists in the mode-matching system. The phase of this residual quadrature signal is used to accomplish and maintain frequency matching between the drive and sense modes.

The drive and sense mode resonance frequencies of the designed gyroscope are tuned to be almost identical to each other with the help of FEM simulations; however, unavoidable fabrication tolerances generally results in mismatched mode frequencies. The main motivation behind the proposed mode-matching system is to automatically tune the sense mode resonance frequency with respect to the drive mode resonance frequency by using the electrostatic tuning capability of the sense mode. The sense mode resonance frequency is adjusted by tuning the electrostatic spring constant of this mode by changing the proof mass voltage, V_{PM}, as described in the equation below

$$\omega_S = \sqrt{\underbrace{\frac{k_{mech}}{m_S}}_{\omega_{S,mech}{}^2} - \frac{N\alpha\varepsilon_0 A}{m_S D_{gap}{}^3} V_{PM}{}^2} \tag{1}$$

where k_{mech} is the mechanical spring constant of the sense mode, m_S is the effective mass of the sense mode, N is the number of varying-gap sense-mode electrodes, α is the fringing field correction factor, ε_0 is the permittivity of free space, A is the overlapped area of the sense-mode electrodes, and D_{gap} is the gap spacing between the capacitive pair of the sense-mode electrodes. It should be noted that there also exists the nominal gap spacing, called anti-gap, between the neighboring capacitor pair of the sense-mode electrodes, which has an effect on the electrostatic spring constant of the sense mode with changing V_{PM}. However, in (1), the effect of the capacitive anti-gap between the neighboring capacitor pair of the sense-mode electrodes is ignored as its effect is approximately 50 times smaller than the effect of the capacitive gap between the capacitive pair of the sense-mode electrodes.

Fig. 2 shows the frequency tuning characteristics of the drive and sense resonance modes of the studied fully-decoupled MEMS gyroscope as a function of V_{PM}. The drive mode resonance frequency of the gyroscope remains constant at 14184 Hz since there are no electrostatic springs acting along the drive mode. The sense mode frequency, on the other hand, can be electronically tuned in the range of 14496 Hz to 12736 Hz by varying V_{PM} from 8 to 15 V. The resonance mode frequencies are perfectly matched at the proof mass potential of 9.33 V for the sensor reported in Fig. 2.

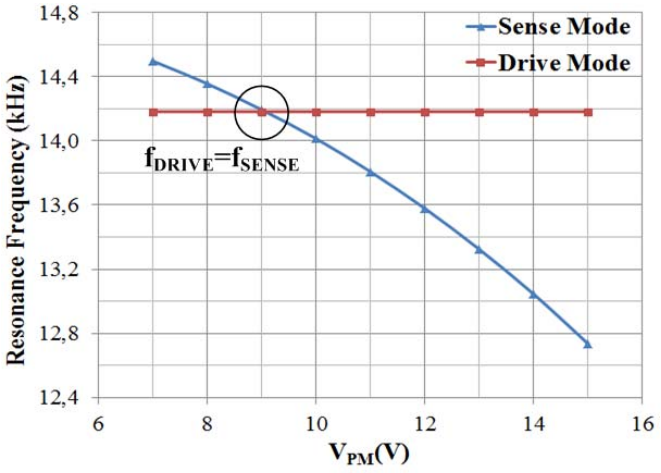

Fig. 2. Frequency tuning characteristics of the drive and sense resonance modes of the studied fully-decoupled MEMS gyroscope as a function of V_{PM}.

A. Design of the Mode-Matching Control Electronics

The proposed automatic mode-matching system operation mainly relies on the phase relationship between the residual quadrature and drive signals in the gyroscope. The sense-mode dynamics of the gyroscope can be modeled as a second order spring-mass-damper system, and then the relation between the existing quadrature displacement (Y_Q) and the corresponding quadrature force (F_Q) can be written as

$$K_S(s) = \frac{Y_Q(s)}{F_Q(s)} = \frac{1/m_S}{\left(s^2 + \frac{\omega_S}{Q_S}s + {\omega_S}^2\right)} \tag{2}$$

where Q_S is the quality factor of the sense mode. Since the phase of the drive signal is always constant at the mode-matching system, the frequency matching condition is achieved by adjusting the phase of the quadrature signal by tuning the resonance frequency of the sense mode. Equation 3 describes the relationship between the phases of the quadrature and drive signals and the former one also being related to the frequencies of the drive and sense modes. If the gyroscope is operated at the drive mode resonance frequency ($s = j\omega_D$) and under the condition of the frequency mismatch between the resonance modes ($\omega_D \neq \omega_S$), the relative phase delay of the quadrature signal with respect to the drive signal is directly derived from (2) as

$$\begin{aligned} \emptyset_0 &= \angle K_S(j\omega_D) = \angle \frac{1/m_S}{-{\omega_D}^2 + j\frac{\omega_D\omega_S}{Q_S} + {\omega_S}^2} \\ &= -\tan^{-1}\left(\frac{1}{Q_S}\frac{\omega_D\omega_S}{(\omega_S^2 - \omega_D^2)}\right) \end{aligned} \tag{3}$$

By replacing the sense mode resonance frequency with (1) in (3), the effective relative phase delay between the quadrature and drive signals can be written as

$$\emptyset(V) = -\tan^{-1}\left(\frac{1}{Q_S}\frac{\omega_D\sqrt{{\omega_{S,mech}}^2 - \frac{N\alpha\varepsilon_0 A}{m_S {D_{gap}}^3}{V_{PM}}^2}}{\left({\omega_{S,mech}}^2 - \frac{N\alpha\varepsilon_0 A}{m_S {D_{gap}}^3}{V_{PM}}^2 - {\omega_D}^2\right)}\right) \tag{4}$$

and the phase shift from the relative phase delay, depending on V_{PM} variation during the mode-matching operation is obtained by

$$\begin{aligned} \Delta\emptyset(V) &= \emptyset_0 - \emptyset(V) \\ &= -\tan^{-1}\left(\frac{1}{Q_S}\frac{\omega_D\sqrt{{\omega_{S,mech}}^2 - \frac{N\alpha\varepsilon_0 A}{m_S {D_{gap}}^3}{V_{PM}}^2}}{\left({\omega_{S,mech}}^2 - \frac{N\alpha\varepsilon_0 A}{m_S {D_{gap}}^3}{V_{PM}}^2 - {\omega_D}^2\right)}\right) \\ &\quad -\tan^{-1}\left(\frac{1}{Q_S}\frac{\omega_D\omega_S}{(\omega_S^2 - \omega_D^2)}\right) \end{aligned} \tag{5}$$

It should be noted from (5) that the phase shift is an even and nonlinear function of V_{PM} due to the electrostatic spring constant shown in (1). Since the phase difference between the quadrature and drive signals is basically used as an indicator of the frequency mismatch amount between the drive and sense modes, the derived phase shift equation is the essential functional element behind the design of the mode-matching control electronics.

Fig. 3 shows the block diagram of the mode-matching control electronics with an analog PI controller that is capable of matching the sense mode resonance frequency to that of the drive mode by automatically changing V_{PM} in a range of only $\pm$2.5V. Such a tuning range is sufficient for the proposed system to compensate for an initial frequency split of up to 1 kHz between the drive and sense modes. In Fig. 3, the quadrature signal is directly picked from the sense pick-off (SP) outputs of the gyroscope through a capacitive preamplifier interface, and the drive signal is directly picked from the drive pick-off (DP) output of the gyroscope through a resistive preamplifier interface. Therefore, there is no phase difference between the drive pick-off (SP) output of the gyroscope and the drive signal, whereas there exists a phase shift of 90°, resulting from the capacitive preamplifier used in the sense-mode, between the sense pick-off (SP) output of the gyroscope and the quadrature signal. The quadrature signal is demodulated with the 90° phase-shifted version of the drive signal (whose phase is selected as the reference phase in the system), and then the output of the demodulator is low-pass filtered to obtain the phase difference information between the quadrature and drive signals. The demodulator together with the low-pass filter equivalently operates as a phase detector. The phase difference information is fed to the PI controller that generates a DC tuning potential, ΔV, to adjust the phase difference between the quadrature and drive signals to a value which is close to the ideally desired value of 0°. Next, the DC tuning potential is applied to the proof mass of the gyroscope after summing it with the fixed DC potential. This fixed DC potential continuously sustains the drive and quadrature signals in the system, and it is required to initiate the mode-matching operation. As a result, the proposed mode-matching closed loop controller tunes the sense mode resonance frequency of the gyroscope with a potential range of $\pm$2.5V till the phase difference between the residual quadrature and drive signals converges to zero, ensuring that mode-matching has been achieved. In this work, the maximum ΔV is limited by the allowed voltage swings of the

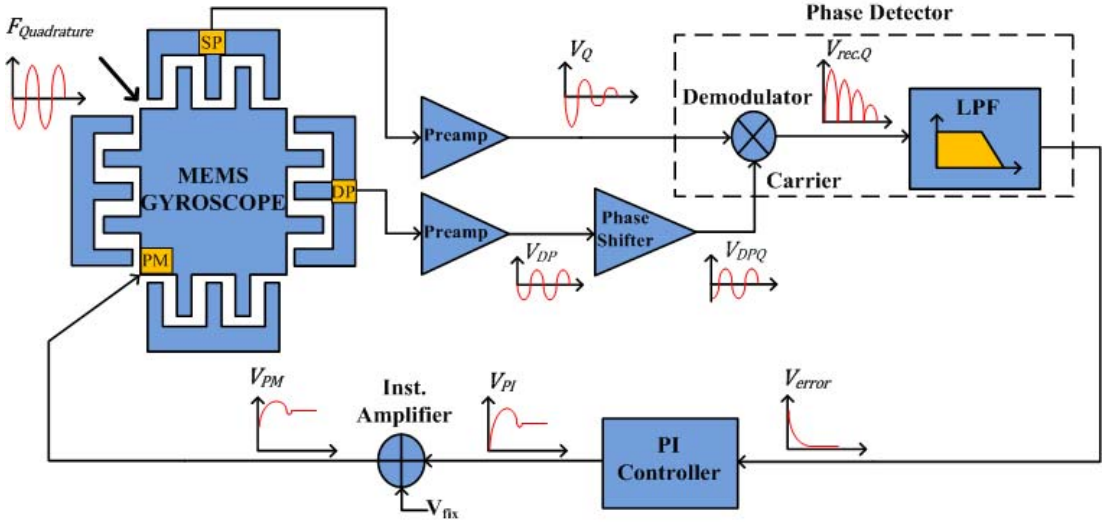

Fig. 3. Block diagram of the mode-matching control electronics that is capable of matching the resonance mode frequencies from maximum 1 kHz separation by changing V_{PM} in a range of only ± 2.5V.

closed-loop feedback control electronics. It should be mentioned here that the phase difference between the quadrature and drive signals never changes from 90° to −90° during the mode-matching operation, and it changes only from 90° to about 0°. Therefore, it is guaranteed that there is no instability in the given mode-matching controller, during the mode-matching operation since the mode-matching control loop never switches from the positive to negative feedback.

There is always a quadrature error in the system due to the fabrication imperfections, and this signal caused by the quadrature error reaches its maximum value at the mode-matched condition due to the boosted sensitivity of the sensor. In the mode-matching system, if the quadrature signal is not substantially cancelled, it does not allow the gyroscope to continuously operate at the mode-matched condition since the sense-mode force-feedback electronics would be saturated then. Note that the sense-mode force-feedback electronics is used only to generate the rate output by cancelling the movement caused by an angular rate input in the sense mode of the gyroscope. Therefore, the quadrature signal should be reduced down to a certain level, in order to perform the mode-matching operation without saturating the sense-mode force-feedback electronics in the proposed system. In this work, the inherent quadrature error resulting from the fabrication imperfections in the gyroscope is cancelled at the mode-matched condition thanks to the quadrature cancellation mechanism including the quadrature cancellation electrodes and electronics with an analog PI controller [14]. Despite the quadrature nulling, there still remains a finite amount of quadrature signal due to constant phase errors in the electronics. The phase errors mostly results from the quadrature cancellation electronics since the electrical feedthrough coupling from drive to sense mode signal, which affects both of the differential sense-mode channel signals as a common-mode signal, is almost-totally eliminated by using a differential readout scheme in the sense-mode of the gyroscope. The amount of the residual quadrature signal due to the phase error in the electronics, which is generally about 0.1 °/s in the proposed system, changes for the different gyroscopes depending on the amount of the inherent quadrature error caused by the fabrication imperfections. Therefore, in order to operate the gyroscope under the mode-matched condition with the known quadrature signal level, the amount of the residual quadrature signal is adjusted to a level of about 1.5 °/s with the help of the closed-loop quadrature cancellation electronics in the proposed mode-matching system. Furthermore, the amount of the residual quadrature signal used to achieve and maintain mode-matching has no major effect on precise matching between the resonance mode frequencies in the system since the system only utilizes the phase information of the quadrature signal. However, the amount of the quadrature signal has a major effect on the bias instability and ARW performances of the gyroscope [14], i.e., if the amount of the residual quadrature signal is increased in the proposed system, the bias instability and ARW performances may significantly degrade for higher quadrature signal levels.

Fig. 4 shows the behavioral model of the mode-matching controller constructed in SIMULINK. In this model, the sense mode dynamics of the gyroscope is partitioned to conversion blocks in order to include some second-order effects like electrostatic spring softening and electrostatic force nonlinearity to accurately estimate the transient behavior of the given mode-matching controller. The parameters of the preamplifier and instrumentation amplifier are inserted to the model inside the displacement-to-voltage conversion block shown in Fig. 4. The SIMULINK model is constructed to observe the transient response characteristics of the mode-matching controller by using the some measured parameters of the system and all measured parameters of one of the studied MEMS gyroscopes, which are summarized in Table I. The PI controller parameters of the mode-matching controller are determined and optimized under the mode-matched condition by using

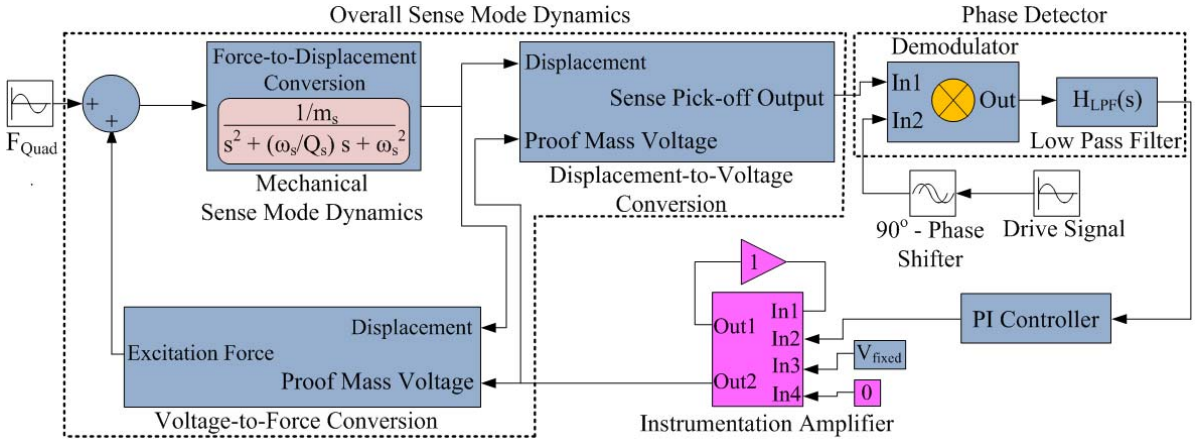

Fig. 4. Behavioral model of the mode-matching controller constructed in SIMULINK.

TABLE I
MEASURED PARAMETERS OF ONE OF THE TESTED MEMS GYROSCOPES

Gyroscope Parameter	Value
Drive Mode Resonance Frequency (f_D)	14182Hz
Drive Mode Quality Factor (Q_D)	33457
Proof Mass Potential (V_{PM})	9.81V
Sense Mode Resonance Frequency (f_S)	14082Hz
Sense Mode Quality Factor (Q_S)	1719
Drive Mode Displacement Amplitude (X_D)	4μm
Sense Mode Capacitance (C_S)	5.6pF
Sense Mode Capacitance Gradient ($\partial C_S/\partial y$)	1.4μF/m
Sense Mode Effective Mass (m_S)	8.43×10^{-8}kg
Proof Mass Frame Effective Mass (m_{PM})	3.41×10^{-8}kg
Number of Sense Electrodes (N)	328
Overlapped Area of Sense Electrodes (A)	$3325\mu m^2$
Capacitive Sense Gap (D_{gap})	2.46μm
Pressure Level Inside the Cavity	~350mTorr

the SIMULINK model of the mode-matching controller. Note that when the resonance mode frequencies of the gyroscope are matched, the second-order sense mode dynamics of the gyroscope can be modeled as a first-order envelope model between the demodulator and instrumentation amplifier, shown in Fig. 4, describing the behavior of the sense-mode resonator in response to possible angular rate inputs at resonance. The first-order sense-mode dynamics of the gyroscope at resonance can be written as

$$H_S(s) = \frac{A_S}{1 + s/\left(\frac{\beta_S}{2}\right)} \tag{6}$$

where A_S is the sense-mode resonance gain of the mode-matched gyroscope, and β_S is the sense-mode bandwidth of the gyroscope. It is seen from (6) that the first-order sense-mode dynamic of the gyroscope introduces a pole located at low-frequency to the system for high-Q sensors [13]. This low-frequency pole together with the pole of the PI controller located at DC (zero frequency) results in a low-unity gain frequency slowing down the transient response characteristics of the mode-matching controller in the order of hundreds of milliseconds. This can lead to a distortion in the proposed system during the mode-matched gyroscope operation for the case when there is any abrupt frequency shift exists between the resonance modes, which may result from the temperature variation in the system. Therefore, in the design of the mode-matching controller, the low-frequency pole coming from the first-order sense-mode dynamics of the gyroscope at resonance is eliminated with a zero adjusted by using the parameters of the PI controller through the pole-zero cancellation method [13]. Hence, the given mode-matching controller operates as expected with a fast transient response characteristic.

Following the optimization of the mode-matching controller, the simulation of the proposed mode-matching system has been carried out by combining the SIMULINK models of the mode-matching controller shown in Fig. 4, reference signal part (drive signal), closed-loop quadrate-cancellation electronics, and sense-mode force-feedback electronics, in order to explicitly observe the transient behavior of the mode-matching controller during the mode-matching operation. In the simulation, the complete model of the studied gyroscope, whose parameters are summarized in Table I, and some measured parameters of the system are used to achieve consistency between the simulation and experiment. Fig. 5 shows the simulated outputs of (a) the tuning potential (ΔV) and (b) the phase detector, obtained during the mode-matching operation for three different initial frequency separations of 50, 100, and 150 Hz. It is clear that the settling time for mode-matching sharply increases for higher initial frequency separation values. This primarily results from the effective gain at the force-to-displacement conversion block shown in Fig. 4. As the initial frequency separation is set to higher values, the effective gain in the start-up period gets smaller, and thus the mode-matching controller requires more time to settle. As observed from Fig. 5(b), when the resonance mode frequencies becomes closer during the mode-matching operation, the phase detector output sharply increases due to the quadrature signal amplification although the phase difference between the drive and quadrature signals is closer to zero. However, when the controller reaches the steady-state condition, the phase difference between the quadrature and drive signals converges to zero, as expected.

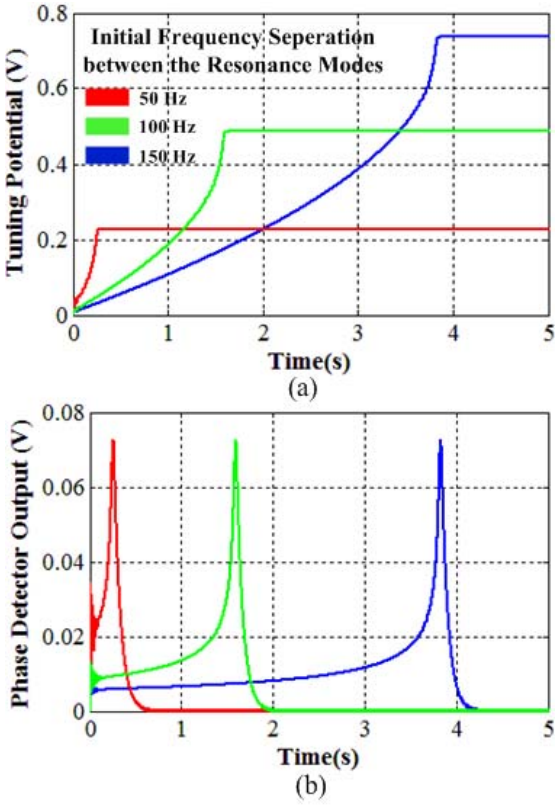

Fig. 5. Simulated outputs of (a) the tuning potential (ΔV) and (b) the phase detector, obtained during the mode-matching operation for three different initial frequency separations of 50, 100, and 150 Hz.

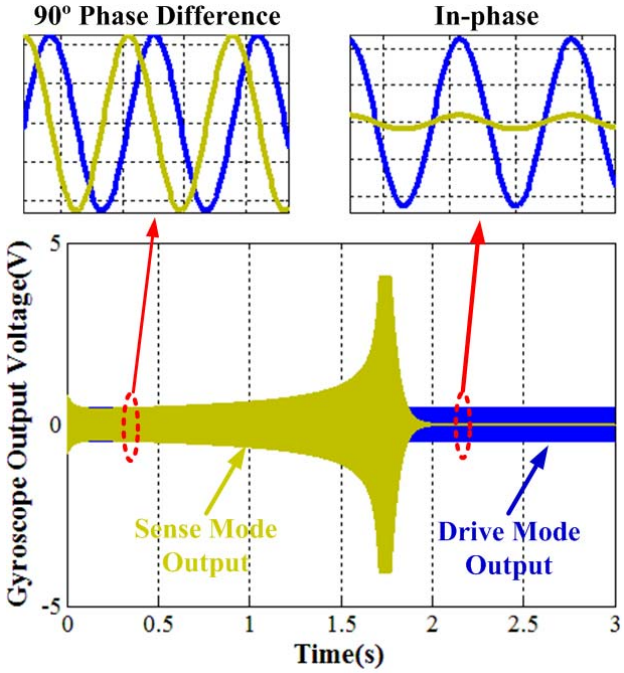

Fig. 6. Transient response of the drive and sense mode outputs of the gyroscope during the mode-matching operation in the absence of an angular rate, for an initial frequency separation of 100 Hz between the resonance modes.

Fig. 6 shows the transient response of the drive and sense mode outputs of the gyroscope during the mode-matching operation in the absence of an angular rate when the initial frequency separation between the drive and sense modes is set to 100 Hz. The magnitude of the quadrature signal in Fig. 6 significantly increases and saturates the sense mode output voltage of the gyroscope until the designed mode-matching controller reaches the steady-state condition. However, when the resonance mode frequencies of the gyroscope are matched, this quadrature signal is drastically minimized to a level of 1.5 °/s with the help of the quadrature cancellation electronics since the phase relationship is now consistent in the closed-loop quadrature cancellation electronics for proper operation. The embedded figures in Fig. 6 are enlarged to capture the phase and amplitude relations between the quadrature and drive signals explicitly. It is seen that the phase difference between the quadrature and drive signals changes from 90° to ideally desired value of 0° during the mode-matching operation. Matching the phases of the residual quadrature and drive signals indicates and guarantees that the frequency matching condition is accomplished.

B. Noise Analysis of the Mechanical Structure and Readout Electronics

The mechanical noise in a vibrating MEMS structure primarily results from the Brownian motion of air molecules [15]. The Brownian force causing this noise motion can be formulated by

$$F_B = \sqrt{4k_B T b} \tag{7}$$

where k_B is the Boltzmann's constant, T is the ambient temperature, and b is the damping constant. The rate-equivalent Brownian (mechanical) noise can be directly calculated for the gyroscope under operation by dividing the Brownian force shown in (7) to the Coriolis force, which can be expressed by

$$\Omega_{\text{rate,mechanical}} = \frac{\sqrt{4k_B T \frac{m_S \omega_S}{Q_S}}}{2m_{PM}\omega_D X_D} \tag{8}$$

where m_S is the effective mass of the sense mode, ω_S is the sense mode resonance frequency, Q_S is the quality factor of the sense mode, m_{PM} is the effective mass of the proof mass frame, ω_D is the drive mode resonance frequency, and X_D is the drive mode displacement amplitude. The rate-equivalent Brownian noise is calculated using (8) in the proposed system by using the measured parameters of one of the tested gyroscopes, which are tabulated in Table I. Note that this is the only mechanical noise. Therefore, the noise coming from the electronics should also be included in order to determine the total rate-equivalent noise ($\Omega_{\text{rate,total}}$) in the gyroscope system, where the rate-equivalent electronic noise ($\Omega_{\text{rate,electronic}}$) is calculated by including the noise contributions of each discrete electronic component in the sense-mode force-feedback electronics. Following the electronic and Brownian noise calculations for the same gyroscope, the total rate-equivalent noise can be found assuming that the electronic and Brownian noises are uncorrelated with each other as follows:

$$\Omega_{\text{rate,total}} = \sqrt{\Omega_{\text{rate,mechanical}}{}^2 + \Omega_{\text{n,electronic}}{}^2} \tag{9}$$

TABLE II
SUMMARY OF THE THEORETICALLY-CALCULATED NOISE VALUES FOR THE MODE-MATCHED AND MISMATCHED (100 HZ) GYROSCOPE OPERATIONS

Parameters	Mismatched (100 Hz)	Mode-Matched
Mechanical Noise Density (°/h/√Hz)	2.26	**2.27**
Electronic Noise Density (°/h/√Hz)	3.71	**0.95**
Total Noise Density (°/h/√Hz)	4.34	**2.46**
ARW(°/√hr)	~0.072	**~0.041**

The total rate-equivalent noise values are calculated using (9) for the same gyroscope operated with the sense-mode force-feedback electronics under the mode-matched and mismatched (100 Hz) conditions, in order to demonstrate the effect of mode-matching on the ARW performance of the gyroscope. Table II shows the summary of the theoretically-calculated noise values for the mode-matched and mismatched (100 Hz) gyroscope operations. In the proposed gyroscope system, the rate-equivalent electronic noise is calculated by dividing the electronic noise coming from the sense-mode force-feedback electronics, which is the same for both the mode-matched and mismatched gyroscope operations, to the rate sensitivity of the sense-mode. At the matched-mode gyroscope operation, the rate sensitivity of the sense-mode is boosted by the mechanical quality factor of the sense mode. The increase in the rate sensitivity improves the SNR of the sensor. Therefore, it is seen from Table II that the rate-equivalent electronic noise of the closed-loop system is highly suppressed under the mode-matched condition, thanks to an improvement in the SNR of the sensor.

C. Bandwidth Characterization of the Proposed Mode-Matching System

Mode-matching improves the performance and increases the sensitivity of the gyroscope in both the closed-loop and open-loop sense-mode operations; however, it leads to a significant bandwidth limitation in the open-loop sense-mode operation as depicted in a previous work [11]. For this case, the system bandwidth is theoretically limited by the mechanical bandwidth of the gyroscope in the open-loop operation. However, in this work, the closed-loop force-feedback electronics is used to eliminate the bandwidth limitation by controlling the sense mode of the gyroscope in the presence of an angular rate input, with the aid of the analog PI controller. The PI controller provides an opportunity to adjust the system bandwidth independently from the mechanical sensor bandwidth, with the use of the pole-zero cancellation method as similarly used in the design of the proposed mode-matching controller.

At the mode-matched case, it is seen from (6) that the sense-mode dynamics of the gyroscope has a low-frequency pole located at $\beta_S/2$ in the proposed high-Q system, where β_S is the sense-mode bandwidth of the gyroscope. This low-frequency pole and the pole of the PI controller at DC (zero frequency) cause a low-unity gain frequency that results in a slow settling characteristic in the sense-mode force-feedback operation. By eliminating the low-frequency pole of the sense-mode dynamics with a zero adjusted by using the parameters of the PI controller through the pole-zero cancellation method [13], the settling characteristic of the force-feedback electronics can be substantially improved. Hence, the rate bandwidth of the system can be extended, independently from the mechanical bandwidth of the sensor, in the closed-loop sense-mode operation compared to the open-loop sense-mode operation. Fig. 7 conceptually shows the effective bandwidth of the closed-loop system can be designed to reach to 50Hz, even with a sensor that has much lower mechanical bandwidth (only 8 Hz for the gyroscope whose operation parameters are listed in Table I).

In the proposed mode-matching system, the design of the sense-mode force-feedback electronics starts with adjusting the ratio between the proportional (K_P) and integral (K_I) gains of the PI controller, in order to eliminate the low-frequency pole coming from the sense-mode dynamics of the mode-matched gyroscope shown in (6). Next, the open loop gain is adjusted to obtain an improved system bandwidth with a sufficient phase margin (>45°) by proportionally changing the amplitudes of K_P and K_I. Fig. 8 shows the simulated bandwidth of the mode-matching system (a) for K_P of 6.6×10^{-3} and K_I of 1×10^{-1}, and (b) for K_P of 5.7×10^{-3} and K_I of 8.6×10^{-2} in the presence of a sinusoidal angular rate input whose frequency ramps from 0 to 60 Hz. The corresponding 3 dB points show that the bandwidth of the mode-matching system can be tuned only by changing the PI controller parameters of the sense-mode force-feedback electronics.

III. TEST RESULTS

Experimental tests have been performed to verify the system bandwidth simulations reported in the previous section. The bias instability and ARW performances of the mode-matched and mismatched (~100 Hz) gyroscope operations and the response of the mode-matching system to temperature variations are analyzed, as well. Fig. 9 shows the MEMS gyroscope module, the test PCB (printed circuit board), and the test setup used in the experiments. The MEMS gyroscope module containing the fabricated MEMS gyroscope and preamplifier electronics is integrated inside a metal hybrid package, which is then vacuum-sealed to reduce the Brownian noise floor of the gyroscope. The gyroscope module is then combined with the closed-loop control electronics on the test PCB.

Fig. 10 shows the measured transient response characteristic of the mode-matching controller output (ΔV) for the initial frequency separation of approximately 100 Hz. From this initial separation, the frequency matching condition between the drive and sense modes is electronically achieved by automatically changing ΔV. It is clearly seen that the measured settling time and the amount of the tuning voltage required for mode-matching of the studied gyroscope are

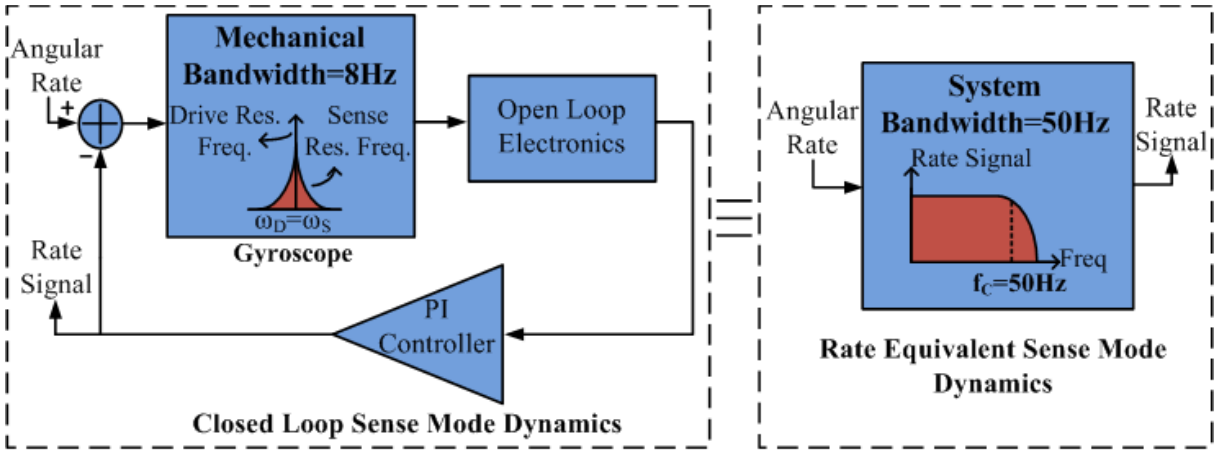

Fig. 7. Closed loop sense mode dynamics with 8 Hz mechanical sensor bandwidth (on the left), and its rate equivalent sense mode dynamics with 50 Hz system bandwidth (on the right). The system bandwidth is extended by adjusting the PI controller parameters, independently from the mechanical sensor bandwidth.

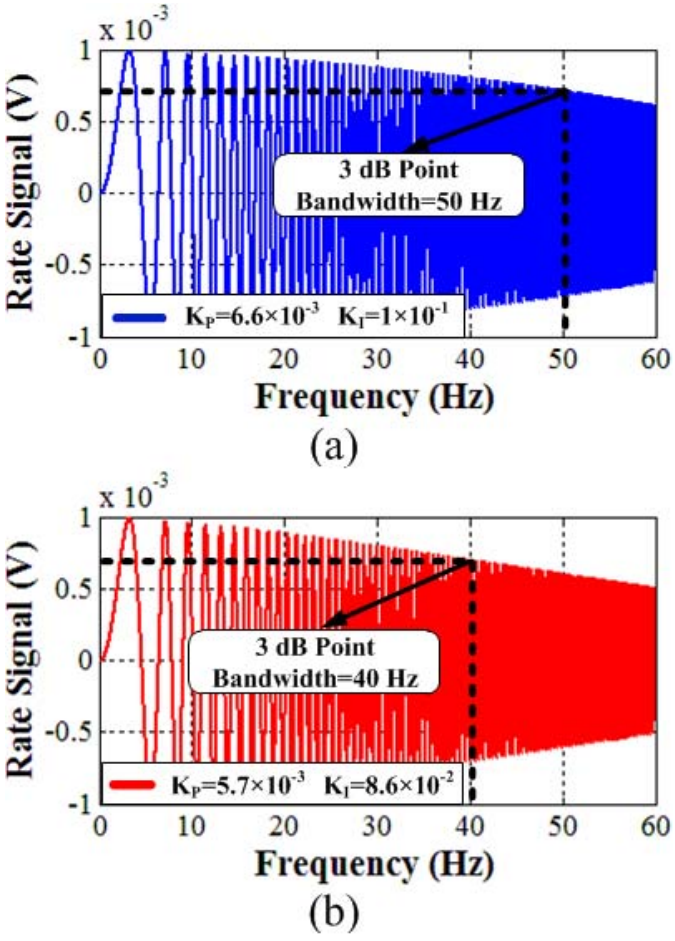

Fig. 8. Simulated bandwidth of the mode-matching system (a) for K_P of 6.6×10^{-3} and K_I of 1×10^{-1}, and (b) for K_P of 5.7×10^{-3} and K_I of 8.6×10^{-2} in the presence of a sinusoidal angular rate input whose frequency ramps from 0 to 60 Hz.

consistent with the simulation result demonstrated in Fig. 5(a). Fig. 11 shows the collection of oscilloscope views showing the frequency separation (Δf) between the drive and sense modes and the phase difference ($\Delta\emptyset$) between the quadrature and drive signals during the mode-matching operation. The phase difference between the quadrature and drive signals directly converges from 90° to about 0.1°, quite close to an ideally desired value of 0°, at the mode-matched condition, as expected. Therefore, there is no instability observed in the mode-matching controller during the tests of the proposed mode-matching system. It is also seen from Fig. 11 that the quadrature signal saturates during the mode-matching operation due to the improved sensitivity of the sensor as the frequency separation between the resonance modes decreases. In the proposed system, the saturated quadrature signal is substantially minimized to a certain level, called residual, thanks to the quadrature cancellation mechanism at the mode-matched condition, and the amount of the residual quadrature signal is automatically-adjusted to be about 1.5 °/s with the aid of the closed-loop quadrature cancellation electronics. Furthermore, the quadrature potentials applied to the quadrature cancellation electrodes for the quadrature minimization result in a resonance frequency shift at the sense-mode during the mode-matching operation. However, the frequency shift caused by these potentials does not affect the mode-matching operation in the system since the given mode-matching controller, operating continuously with the quadrature cancellation electronics, automatically tunes the sense mode resonance frequency by utilizing the phase relationship between the quadrature and drive signals during the mode-matching operation. It has also been calculated that the spring-softening effect caused by the quadrature potentials on the sense mode resonance frequency is less than 1/30 of that generated by the varying-gap sense-mode electrodes which have no major effect on the sense mode resonance frequency in this system.

In the proposed mode-matching system, it is crucial that the phase error between the quadrature and drive signals should be kept as small as possible, in order to get the highest gyro performance under the mode-matched condition since the given mode-matching controller utilizes the phase relationship between these signals to achieve and maintain mode-matching. In the system, the phase error between the quadrature and drive signals mostly results from the readout

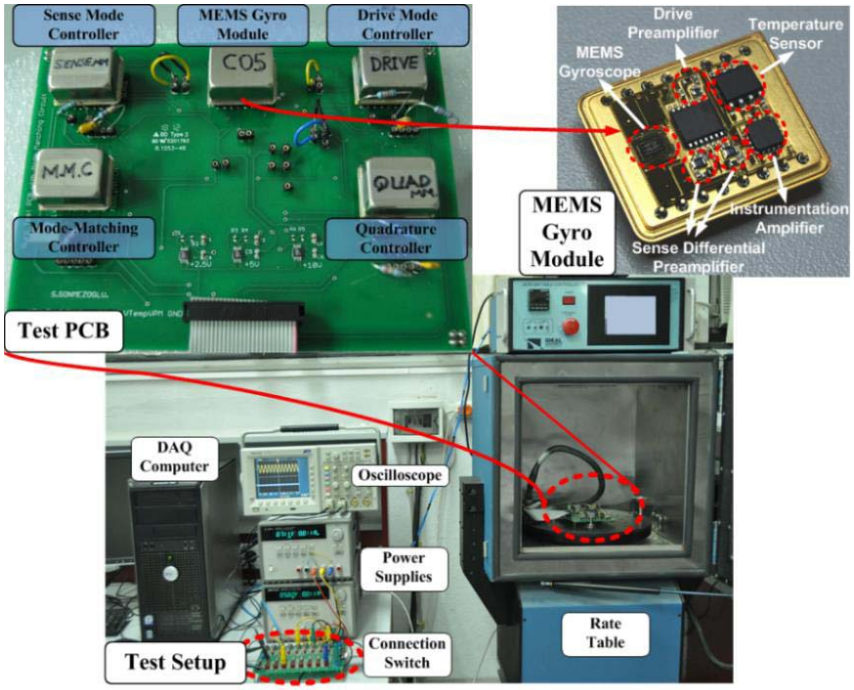

Fig. 9. Experimental test setup of the mode-matching system. (Inset) Test PCB including the complete gyroscope system and MEMS gyroscope module containing the MEMS gyroscope and preamplifier electronics.

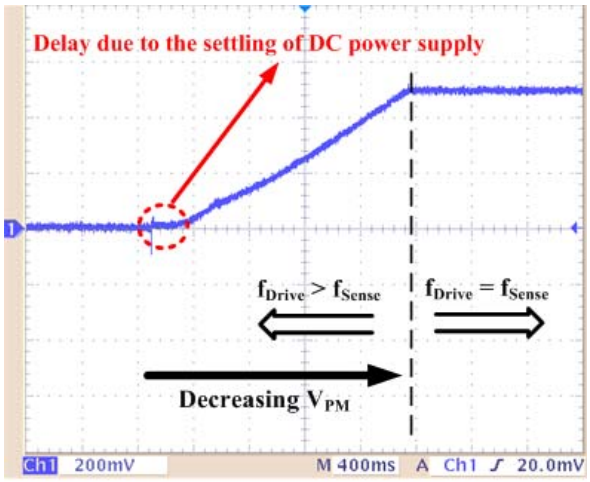

Fig. 10. Oscilloscope view of the transient response characteristic of the mode-matching controller output (ΔV) for the initial frequency separation of approximately 100 Hz.

electronics since the electrical feedthrough coupling from drive to sense mode signal is almost-totally suppressed by using the differential readout scheme in sense-mode of the gyroscope. The phase error between the residual quadrature and drive signals can be directly observed from Fig. 11(c), and it is measured to be about 0.1° for the proposed system. In matched-mode operation, the proposed system achieves and maintains mode-matching with an error less than 10ppm/Hz frequency separation between the drive and sense modes (within the precision of the measurement setup) for the phase error of about 0.1°, where the drive and sense mode quality factors of the gyroscopes are about 33000 and 1700, respectively.

A. System Bandwidth Measurement

Fig. 12 shows the frequency response of the mode-matching system that is experimentally measured up to the utilized rate table limit of 42 Hz, and then overlapped with the simulated data. It is clearly seen from Fig. 12 that the measured and simulated data are almost-totally consistent with each other in the frequency range of 42 Hz, which evidently indicate and verify that the system bandwidth can be estimated as 50 Hz by extrapolating the simulation results.

Fig. 13 shows the measured sense mode output in response to two different angular rate inputs. These inputs have the same amplitude of 2π °/s with the frequency of 20 and 40 Hz, which are observed as sidelobes with the amplitude of about 18.1 and 20.1 mV_{rms}, respectively. The amplitude reduction of the sidelobes is caused by the system bandwidth characteristic at an elevated applied angular rate input frequency. The central peak is the measured sum of the in-phase and quadrature offset signals, which are always located at the drive mode resonance frequency. The amplitude of the central peak is about 6 mV_{rms} corresponding to 1.63 °/s, which is quite small compared to the amplitude of the sidelobes. This also ensures the functionality of our mode-matching system because if it does not work properly then the quadrature signal would not be cancelled as a result of the phase inconsistency in the closed-loop quadrature cancellation electronics.

B. Performance Results

The performances of the studied gyroscopes are experimentally determined at room temperature for a drive displacement of 4μm under mismatched (~100Hz) and mode-matched conditions by using the Allan variance technique. During the

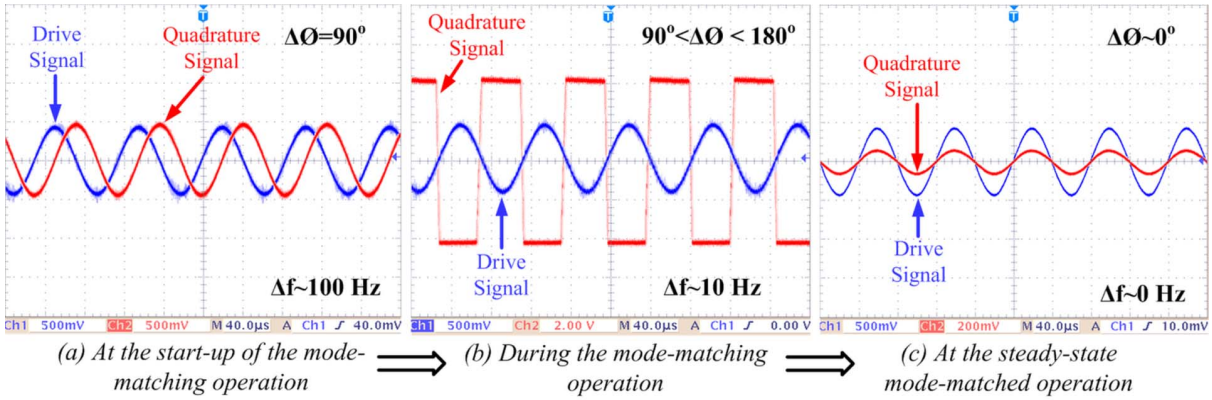

Fig. 11. Collection of oscilloscope views showing the frequency separation (Δf) between the drive and sense modes and the phase difference (ΔØ) between the quadrature and drive signals during the mode-matching operation.

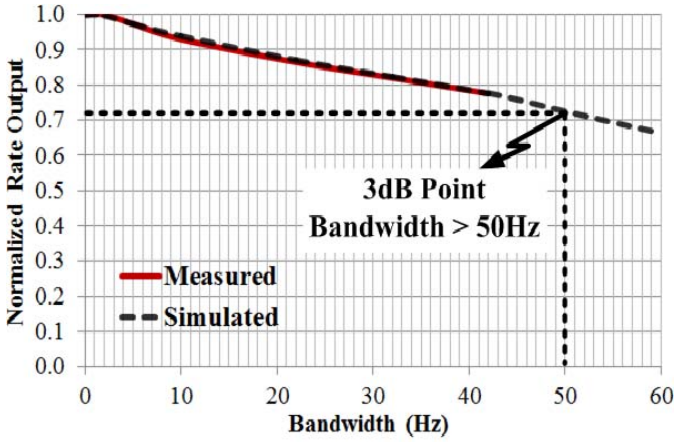

Fig. 12. Frequency response of the mode-matching system that is measured up to 42 Hz, and then overlapped with the simulated data.

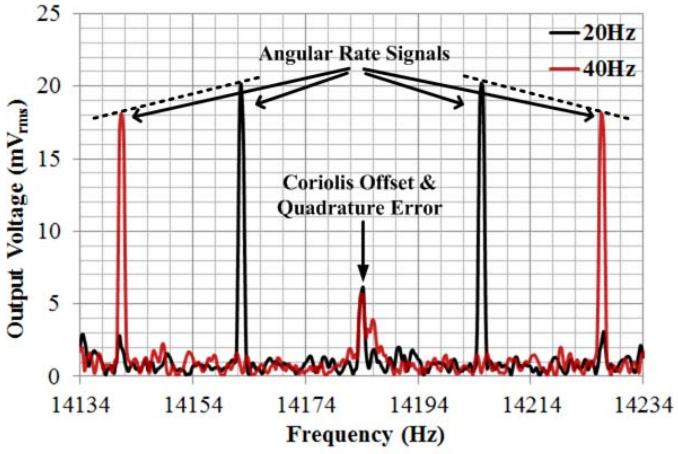

Fig. 13. Measured sense mode output in response to sinusoidal angular rate inputs with amplitudes of 2π °/s and frequencies of 20 and 40 Hz.

TABLE III
TEST RESULTS OF DIFFERENT GYROSCOPES UNDER MISMATCHED (~100 HZ) AND MODE MATCHED CONDITIONS

Performance Parameters	Mismatched (~100 Hz) Mode		Matched Mode	
Gyro ID	#1	#2	#1	#2
ARW (°/√hr)	0.072	0.043	**0.041**	**0.036**
Bias Instability (°/hr)	3.2	2.6	**1.1**	**1.6**
V_{PM} (V)	9.81	10.15	**9.33**	**9.55**
Scale Factor (mV/°/s)	12.9	13.6	**14.2**	**15.4**

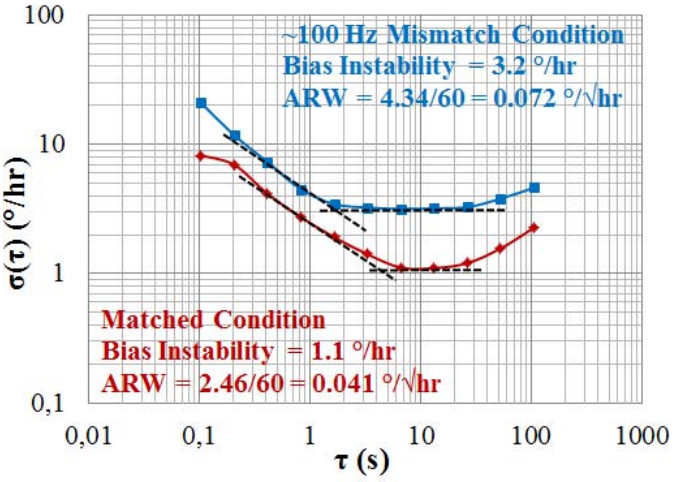

Fig. 14. Allan variance graphs of Gyro#1 with a 1.1°/hr bias instability and 0.041°/√hr ARW, close to the estimated theoretical Brownian noise limit of 0.038 °/√hr.

performance tests, the zero-rate output (ZRO) data of the tested gyroscopes is collected for a period of 15 min with a sampling frequency of 5 kHz. Table III illustrates the test results of two different gyroscopes, showing ARW, bias instability, DC proof mass voltages, and scale factors for mismatched (~100Hz) and mode-matched conditions. Test results demonstrate that the bias instability and ARW performances are substantially improved up to about 2.9 and 1.8 times, respectively, with mode-matching. The performance improvement is substantially limited by the mechanical noise of the sensor, which is impossible to be improved by mode-matching.

Fig. 14 presents the Allan variance graphs of one of the tested gyroscopes (Gyro#1) under the mismatched (~ 100Hz) and mode-matched conditions. The bias instability and ARW performances of the gyroscope are measured to be 1.1 °/hr and 0.043 °/√hr, respectively, under the mode-matched

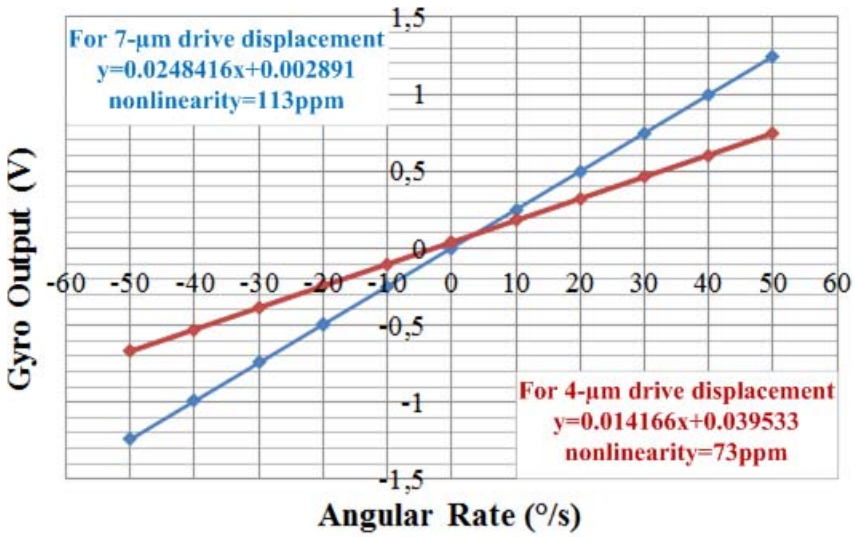

Fig. 15. Output response of the mode-matched gyroscope (Gyro#1) as a function of the applied rate for 4μm and 7μm drive displacement values.

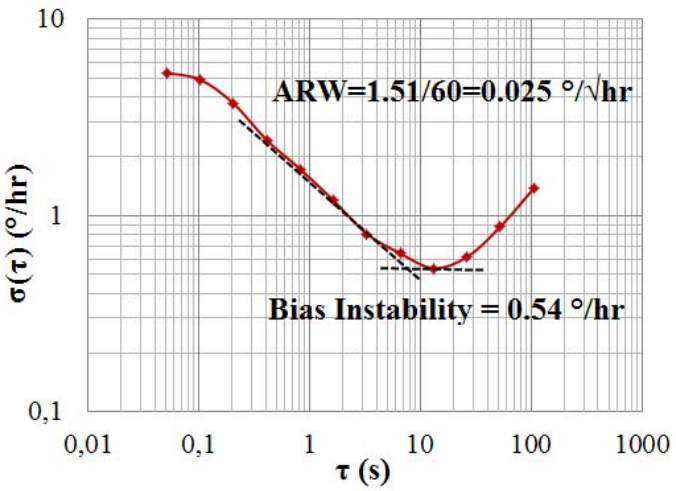

Fig. 16. Allan variance graph of Gyro#1 with an exceptional performance, showing the bias instability of 0.54 °/hr and ARW of 0.025 °/$\sqrt{}$hr. These results are achieved with the increased drive displacement (7μm) and the mode-matched operation.

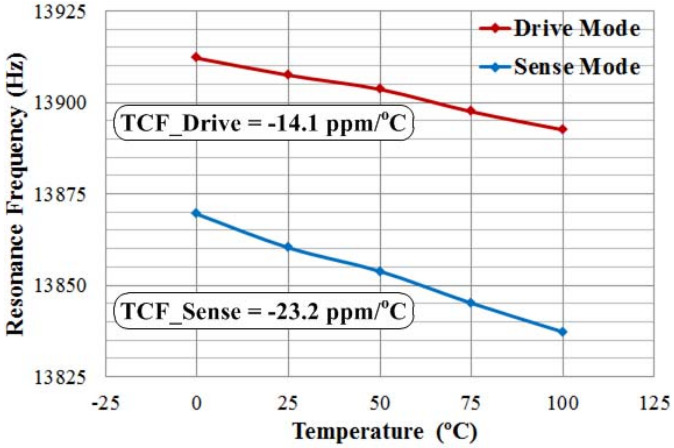

Fig. 17. Individual unmatched resonance mode frequencies of Gyro#1 as a function of temperature.

condition. The measured ARW performance is quite close to the estimated theoretically-calculated Brownian noise limit of 0.038 °/$\sqrt{}$hr for this gyroscope, with mode-matching. This verifies and indicates that the electronic noise of the closed-loop system is significantly suppressed with mode-matching.

In order to push the performance of the gyroscope to its limits, the rate equivalent Brownian noise ($\Omega_{rate,mechanical}$) in (8) should be reduced either by increasing the sense mode quality factor (Q_S) or the drive displacement (X_D) since the remaining parameters are already fixed by the mechanical design of the gyroscope. Increasing the drive displacement is easier compared to improving the sense mode quality factor, which is limited by the pressure inside the sealed gyroscope module.

Fig. 15 shows the output response of the mode-matched gyroscope (Gyro#1) as a function of the applied rate fr 4μm and 7μm drive displacement values. It is clear that the scale factor increased from 14.2mV/°/s for 4μm drive displacement to 24.8mV/°/s for 7μm drive displacement without causing a significant degradation in the linearity of Gyro#1.

Fig. 16 shows Allan variance graph of Gyro#1 with an exceptional performance, showing the bias instability of 0.54 °/hr and ARW of 0.025 °/$\sqrt{}$hr that is very close to the theoretically-calculated Brownian noise of 0.022 °/$\sqrt{}$hr. This result is accomplished with the increased drive displacement (7μm) under the mode-matched condition. It is obvious that increasing the drive displacement by a factor of 1.75 reduces the ARW performance of the sensor by a factor of about 1.75. The measured gyro performance for 7μm drive displacement makes the proposed mode-matching system substantially better than most of the commercially available MEMS gyroscopes [16].

C. Temperature Behavior of the Mode-Matching System

In order to ensure reliable and high gyro performance, it is crucial that the frequency matching condition is maintained under the changing temperature condition. The studied gyroscope was tested to observe the effects of temperature on the resonance mode frequencies. Fig. 17 shows the

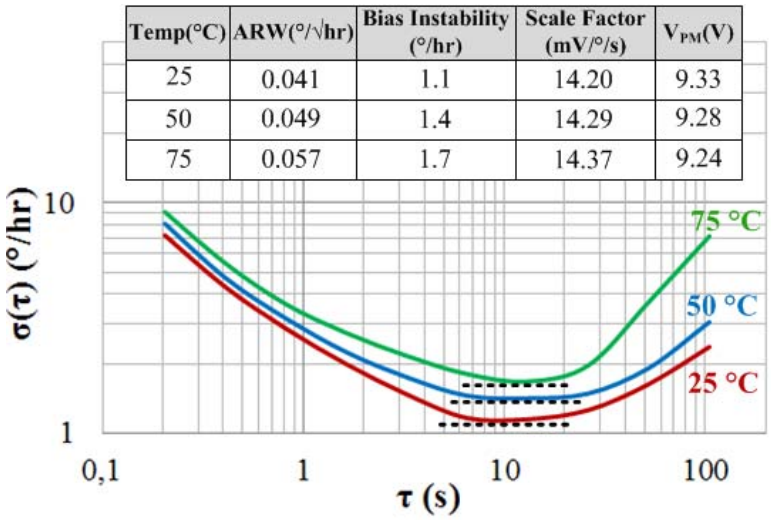

Fig. 18. Allan variance graphs of Gyro#1 obtained at temperatures of 25 °C, 50 °C, and 75 °C.

individual unmatched resonance mode frequencies of Gyro#1 as a function of temperature. Temperature coefficients of the drive and sense mode resonance frequencies (TCF) are measured to be −14.1 ppm/°C and −23.2 ppm/°C, respectively, in a temperature range from 0 °C to 100 °C. The difference between TCF of the drive and sense modes is believed to be related to the gyroscope structure.

Maintaining the automatic mode-matched condition over temperature is verified experimentally for the proposed gyroscope. Here, the mode-matching system is operated in a temperature range from 0 °C to 100 °C without turning off the system throughout the test. As observed from Fig. 17, the TCF of the drive and sense modes are quite different from each other, which directly indicates that the resonance mode frequencies should be re-tuned with changing temperature during the gyroscope operation, in order to maintain mode-matching in the system. Even with different TCF of the drive and sense modes, the proposed mode-matching system automatically maintains the frequency matching condition by continuously tuning V_{PM} with respect to the phase relationship between the residual quadrature and drive signals. However, it should be noted here that the V_{PM} variation with changing temperature causes a scale factor variation as inversely proportional with the square of V_{PM} in the proposed system since both the drive and sense mode dynamics of the gyroscope are simultaneously affected from the V_{PM} variation during the mode-matched gyroscope operation [17].

The Allan variance analysis is performed at three constant temperature settings when operating the gyroscope under the mode-matched condition with a 4μm drive displacement. The ZRO and scale factor data are collected for the Allan variance analysis at temperatures of 25 °C, 50 °C, and 75 °C. In each temperature setting, the thermal equilibrium is satisfied between the ambient and device before recording the ZRO and scale factor data. To achieve the thermal equilibrium, the gyroscope is allowed to attain to a desired temperature for a minimum period of 3 hours. Fig. 18 shows the Allan variance graphs of Gyro#1 obtained at temperatures of 25 °C, 50 °C, and 75 °C. The table embedded to Fig. 18 demonstrates ARW, bias instability, scale factors, and DC proof mass voltages obtained at temperatures of 25 °C, 50 °C, and 75 °C for Gyro#1 operated under the mode-matched condition. The gyroscope demonstrates the best performance at 25 °C, thanks to the value of sense mode quality factor, Q_S, showing the performance of 0.041 °/$\sqrt{}$hr ARW and 1.1 °/hr bias instability with mode-matching. The ARW and bias instability performances degrade for higher temperatures. The degradation in ARW is primarily caused by an increase in the mechanical Brownian noise of the gyroscope resulting from a drop in Q_S. Table IV summarizes the measured sense mode quality factors of Gyro#1 for temperatures of 25 °C, 50 °C, and 75 °C. It is observed that an increase in temperature leads to the quality factor degradation at the sense mode of the gyroscope. This is mainly attributed to the energy-loss mechanisms declared in [18]. The bias instability increases to 1.7 °/hr at 75 °C. This is believed to be related to the reduction in sensitivity of the sensor at elevated temperatures. The reduction in sensor sensitivity also results from the sense mode quality factor degradation.

TABLE IV
MEASURED SENSE MODE QUALITY FACTORS OF GYRO#1 FOR TEMPERATURES OF 25 °C, 50 °C, AND 75 °C

Temperature (°C)	Sense Mode Quality Factor (Q_S)
25	1719
50	1365
75	1043

IV. CONCLUSION

This paper proposes the usage of the phase relationship between the residual quadrature and drive signals in the gyroscope in order to achieve and maintain automatic frequency matching between the resonance modes. Tests performed

under the mismatched (∼100 Hz) and mode-matched conditions for 4μm drive displacement show that the bias instability and ARW performances of the gyroscope are improved up to 2.9 and 1.8 times, respectively, with mode-matching in the closed loop system having a bandwidth of 50 Hz. In order to push the performance of the studied gyroscope to its limits, the amplitude of the drive displacement is increased from 4μm to 7μm. With an increased drive displacement amplitude (7μm), it has been experimentally shown that the mode-matched gyroscope shows an outstanding performance, reaching down to a very low bias instability of 0.54 °/hr and an ARW of 0.025 °/$\sqrt{}$hr at room temperature. The measured ARW is very close to the theoretical Brownian noise limit of 0.022 °/$\sqrt{}$hr, which verifies that the electronic noise in the closed-loop system is highly-suppressed with mode-matching. Furthermore, the proposed mode-matching system is operated in a temperature range from 0 °C to 100 °C without turning off the system throughout the test to experimentally shown that the mode-matching is maintained over a wide temperature range, even though TCF of the drive and sense modes are quite different from each other.

ACKNOWLEDGMENT

Authors would like to thank Mr. Erdinc Tatar and Mr. Burak Eminoglu for their efforts during the tests of the mode-matching system.

REFERENCES

[1] N. Yazdi, F. Ayazi, and K. Najafi, "Micromachined inertial sensors," *Proc. IEEE*, vol. 86, no. 8, pp. 1640–1659, Aug. 1998.

[2] M. Lutz, W. Golderer, J. Gerstenmeier, J. Marek, B. Maihofer, S. Mahler, *et al.*, "A precision yaw rate sensor in silicon micromachining," in *9th Int. Conf. Solid-State Sens. Actuators Tech. Dig.*, vol. 2. Chicago, IL, USA, Jun. 1997, pp. 847–850.

[3] A. Sharma, F. M. Zaman, B. V. Amini, and F. Ayazi, "A high-Q in-plane SOI tuning fork gyroscope," in *Proc. IEEE Sens.*, vol. 1. Vienna, Austria, Oct. 2004, pp. 467–470.

[4] F. Ayazi and K. Najafi, "A HARPSS polysilicon vibrating ring gyroscope," *J. Microelectromech. Syst.*, vol. 10, no. 2, pp. 169–179, Jun. 2001.

[5] M. F. Zaman, A. Sharma, Z. Hao, and F. Ayazi, "A mode-matched silicon-yaw tuning-fork gyroscope with sub-degree-per-hour allan deviation bias instability," *J. Microelectromech. Syst.*, vol. 17, no. 6, pp. 1526–1536, Dec. 2008.

[6] T. Remtema and L. Lin, "Active frequency tuning for microresonators by localized thermal stressing effects," *Sens. Actuators A, Phys.*, vol. 91, no. 3, pp. 326–332, Jul. 2001.

[7] D. Joachim and L. Lin, "Characterization of selective polysilicon deposition for MEMS resonator tuning," *J. Microelectromech. Syst.*, vol. 12, no. 2, pp. 193–200, Apr. 2003.

[8] M. A. Abdelmoneum, M. M. Demirci, L. Yu-Wei, and C. T. C. Nguyen, "Location-dependent frequency tuning of vibrating micromechanical resonators via laser trimming," in *Proc. IEEE Int. Freq. Control Symp. Exposit.*, Montreal, Canada, Aug. 2004, pp. 272–279.

[9] H. Wu, "System architecture for mode-matching a MEMS gyroscope," M.S. thesis, Dept. Electr. Eng. Comput. Sci., Massachusetts Inst. Technol., Cambridge, MA, USA, Jun. 2009.

[10] C. D. Ezekwe and B. E. Boser, "A mode-matching $\Delta\Sigma$ closed-loop vibratory-gyroscope readout interface with a 0.004Å°/s/$\sqrt{}$Hz noise floor over a 50 Hz band," *J. Solid-State Circuits*, vol. 43, no. 12, pp. 3039–3048, Dec. 2008.

[11] A. Sharma, M. F. Zaman, M. Zucher, and F. Ayazi, "A 0.1°/HR bias drift electronically matched tuning fork microgyroscope," in *Proc. 21st Int. Conf. MEMS*, Tucson, AZ, USA, Jan. 2008, pp. 6–9.

[12] S. Sonmezoglu, S. E. Alper, and T. Akin, "An automatically mode-matched MEMS gyroscope with 50 Hz bandwidth," in *Proc. 25th Int. Conf. MEMS*, Paris, France, Feb. 2012, pp. 523–526.

[13] B. Eminoglu, S. E. Alper, and T. Akin, "An optimized analog drive-mode controller for vibratory MEMS gyroscopes," in *Proc. Int. Conf. Eurosensors*, vol. 25. Athens, Greece, Sep. 2011, pp. 1309–1312.

[14] E. Tatar, S. E. Alper, and T. Akin, "Effect of quadrature error on the performance of a fully-decoupled MEMS gyroscopes," in *Proc. 24th Int. Conf. MEMS*, Cancun, Mexico, Jan. 2011, pp. 569–572.

[15] T. B. Gabrielson, "Mechanical-thermal noise in micromachined acoustic and vibration sensors," *IEEE Trans. Electron Devices*, vol. 40, no. 5, pp. 903–909, May 1993.

[16] M. S. Weinberg and A. Kourepenis, "Error sources in in-plane silicon tuning-fork MEMS gyroscopes," *J. Microelectromech. Syst.*, vol. 15, no. 3, pp. 479–491, Jun. 2006.

[17] S. Sonmezoglu, S. E. Alper, and T. Akin, "A high performance automatic mode-matched MEMS gyroscope with an improved thermal stability of the scale factor," in *Proc. Int. Conf. Transducers*, Barcelona, Spain, Jun. 2013, pp. 2519–2522.

[18] B. Kim, M. A. Hopcroft, R. N. Candler, C. M. Jha, M. Agarwal, R. Melamud, *et al.*, "Temperature dependence of quality factor in MEMS resonators," *J. Microelectromech. Syst.*, vol. 17, no. 3, pp. 755–766, Jun. 2008.

Soner Sonmezoglu received the B.S. and M.S. degrees (with high honors) in electrical and electronics engineering from Middle East Technical University (METU), Ankara, Turkey, in 2010 and 2012, respectively. He is currently working toward the Ph.D. degree in electrical and computer engineering, University of California, Davis, CA, USA. He was a Research Assistant with the Micro-Electro-Mechanical Systems Research and Applications Center, METU, between 2010 and 2013. He has been a Graduate Research Assistant with the University of California, Davis, since 2013. His research interests include MEMS, inertial sensors, capacitive interface circuits, and analog closed-loop control.

Said Emre Alper (M'10) was born in Ankara, Turkey, in 1976. He received the B.S., M.Sc., and Ph.D. degrees in electrical and electronics engineering (with high honors) from the Middle East Technical University (METU), Ankara, Turkey, in 1998, 2000, and 2005, respectively. From 1998 to 2005, he was a Research Assistant at the MEMS-VLSI Research Group, Department of Electrical and Electronics Engineering, METU, where he was employed as a Senior Research Scientist and Instructor until 2008. Since 2008, he continued research at the METU-MEMS Research and Applications Center, where he has been the Deputy Director since 2009. He is also the Technical Leader of the Inertial Sensors Research and Technology Development Group at the METU-MEMS Center.

Major research interests of Dr. Alper's include capacitive MEMS inertial sensors, capacitive interface circuits, analog closed-loop control, various microfabrication technologies, packaging and testing of MEMS inertial sensors, and also the hybrid system design.

Dr. Alper received the METU Thesis of the Year Award in 2000 and 2005 for his M.Sc. thesis and Ph.D. dissertation, respectively, which were awarded by the Prof. Mustafa N. Parlar Education and Research Foundation. He is the first author of the symmetric and decoupled gyroscope design, which won the first prize award in the operational designs category of the International Design Contest organized by the Design, Automation, and Test (DATE) Conference in Europe and CMP in March 2001. He is also the first author of the tactical-grade symmetrical and decoupled microgyroscope design, which won the third-prize award, among 132 MEMS designs from 24 countries and 25 states across the US, in the international 3-D MEMS Design Challenge, organized by MEMGEN Corporation (currently Microfabrica, Inc.) in June 2003. Dr. Alper is the author or co-author of more than 30 technical papers published in various international conference proceedings and journals.

Tayfun Akin was born in Van, Turkey, in 1966. He received the B.S. degree in electrical engineering with high honors from Middle East Technical University (METU), Ankara, Turkey, in 1987, and went to the USA in 1987 for his graduate studies with a graduate fellowship provided by NATO Science Scholarship Program through the Scientific and Technical Research Council of Turkey (TUBITAK). He received the M.S. degree in 1989 and the Ph.D. degree in 1994 in electrical engineering, both from the University of Michigan, Ann Arbor MI, USA. In 1995, 1998, and 2004, he was employed as an Assistant Professor, Associate Professor, and Professor, respectively, in the Department of Electrical and Electronics Engineering at METU. He is also the Director of the METU-MEMS Center. His research interests include MEMS, microsystems technologies, uncooled infrared detectors and readout circuits, inertial microsensors, silicon-based integrated sensors and transducers, and analog and digital integrated circuit design.

He has served in various MEMS, eurosensors, and transducers conferences as a Technical Program Committee Member. He was the co-chair of The 19th IEEE International Conference of MEMS (MEMS 2006) held in Istanbul, and he was the co-chair of the Steering Committee of the IEEE MEMS Conference in 2007. He is a Steering Committee Member of The 18th Int. Conf. on Solid-State Sensors, Actuators and Microsystems (Transducers'2015). He is the winner of the First Prize in Experienced Analog/Digital Mixed-Signal Design Category at the 1994 Student VLSI Circuit Design Contest, organized and sponsored by Mentor Graphics, Texas Instruments, Hewlett-Packard, Sun Microsystems, and Electronic Design Magazine. He is the co-author of the symmetric and decoupled gyroscope project, which won the First Prize award in the operational designs category of the international design contest organized by the DATE Conference and CMP in March 2001. He is also the co-author of the gyroscope project, which won the Third Prize award in the 3-D MEMS Design Challenge organized by MEMGen Corporation (currently, Microfabrica).